

Emergent topological spin structures in the centrosymmetric cubic perovskite SrFeO₃

S. Ishiwata^{1,2,3,*}, T. Nakajima,⁴ J.-H. Kim,⁵ D. S. Inosov,^{5,6} N. Kanazawa,¹ J. S. White,⁷ J. L. Gavilano,⁷ R. Georgii,^{8,9} K. M. Seemann,^{8,9} G. Brandl,⁹ P. Manuel,¹⁰ D. D. Khalyavin,¹⁰ S. Seki,⁴ Y. Tokunaga,¹¹ M. Kinoshita,¹ Y. W. Long,^{4,12} Y. Kaneko,⁴ Y. Taguchi,⁴ T. Arima,^{4,11} B. Keimer,⁵ and Y. Tokura^{1,4}

¹Department of Applied Physics and Quantum-Phase Electronics Center, University of Tokyo, Hongo, Tokyo 113-8656, Japan

²JST-PRESTO, Kawaguchi, Saitama 332-0012, Japan

³Division of Materials Physics, Graduate School of Engineering Science, Osaka University, Toyonaka, Osaka 560-8531, Japan

⁴RIKEN Center for Emergent Matter Science, Wako, Saitama 351-0198, Japan

⁵Max-Planck-Institut für Festkörperforschung, D-70569 Stuttgart, Germany

⁶Institut für Festkörper- und Materialphysik, TU Dresden, D-01069 Dresden, Germany

⁷Laboratory for Neutron Scattering and Imaging, Paul Scherrer Institut, CH-5232 Villigen, Switzerland

⁸Physik Department E21, Technische Universität München, D-85748 Garching, Germany

⁹Heinz Maier-Leibnitz Zentrum, Technische Universität München, D-85748 Garching, Germany

¹⁰ISIS Facility, STFC Rutherford Appleton Laboratory, Chilton, Didcot, Oxfordshire OX11 0QX, United Kingdom

¹¹Department of Advanced Materials Science, University of Tokyo, Kashiwa 277-8561, Japan

¹²Beijing National Laboratory for Condensed Matter Physics, Institute of Physics, Chinese Academy of Sciences, Beijing 100190, China



(Received 2 December 2019; accepted 25 February 2020; published 6 April 2020)

The skyrmion crystal (SkX) characterized by a triple- \mathbf{q} helical spin modulation has been reported to be a unique topological state that competes with the single- \mathbf{q} helimagnetic order in noncentrosymmetric materials with Dzyaloshinskii-Moriya (DM) interactions. Here, we report the discovery of a rich variety of multiple- \mathbf{q} helimagnetic spin structures in the centrosymmetric cubic perovskite SrFeO₃ without DM interactions. On the basis of neutron diffraction measurements, we have identified two types of robust multiple- \mathbf{q} spin structures that appear in the absence of external magnetic fields: an anisotropic double- \mathbf{q} spin spiral and an isotropic quadruple- \mathbf{q} spiral hosting a three-dimensional lattice of topological singularities. The present system not only diversifies the family of SkX host materials but furthermore provides an experimental missing link between centrosymmetric lattices and topological helimagnetic order. It also offers perspectives for integration of SkXs into oxide electronic devices.

DOI: [10.1103/PhysRevB.101.134406](https://doi.org/10.1103/PhysRevB.101.134406)

I. INTRODUCTION

The discovery of novel magnetic structures has the potential to open new fields in condensed-matter physics. This is exemplified by magnetic skyrmions with a vortexlike spin configuration, which has led to a multitude of possible applications of topological spin textures in spintronics [1–5]. Highly symmetric crystal lattices allow magnetically ordered states with different equivalent propagation vectors \mathbf{q} , and complex mesoscopic superstructures can emerge from superpositions of several such degenerate states. The “skyrmion crystal” (SkX), viewed as a multi- \mathbf{q} superposition of magnetic skyrmions spin helices, has garnered particular recent attention because of its intriguing connection to topological spin and charge transport phenomena [6–9].

So far, SkXs have mostly been reported for noncentrosymmetric lattices, with details depending on the symmetry of the underlying crystal lattice, the magnetic anisotropy, and the relative strength of the competing interactions, i.e., the ferromagnetic exchange interaction and the Dzyaloshinskii-Moriya (DM) interaction [5]. Three types of two-dimensional SkX characterized by multiple coplanar \mathbf{q} vectors have been

reported: (i) a Bloch-type SkX formed by superposing three proper-screw spin modulations, which has been found in chiral helimagnets such as B20 compounds (MnSi, FeGe, etc.) [3,10–12], Cu₂OSeO₃ [13], and Co-Zn-Mn alloys [14], (ii) a Néel-type SkX formed by three cycloidal spin modulations found in polar helimagnets, like GaV₄(S,Se)₈ and VOSe₂O₅ [15–18], and (iii) an antiskyrmion crystal formed by three spiral spin modulations found in a Mn-Pt-Sn inverse Heusler compound with $D2d$ symmetry [19]. Note that the DM interaction induced at a surface or interface can stabilize the Néel-type SkX as seen in a Fe monolayer on an Ir(111) surface [20]. Recently, a three-dimensional topological spin structure generated by triple- \mathbf{q} vectors that are orthogonal to each other was identified in the B20 compound MnGe with the DM interaction [21]. This spin structure has hedgehog and antihedgehog singularities bridged by intervening skyrmion strings, where the associated emergent magnetic monopole and antimonopole manifest themselves as a source of anomalous magnetotransport phenomena [7,22].

In noncentrosymmetric helimagnets, the DM interaction originating from spin-orbit coupling apparently plays an important role in the formation of a SkX by selecting both the helicity and vorticity for each skyrmion [7,21,22]. On the other hand, the emergence of SkXs has been theoretically predicted also to occur in centrosymmetric helimagnets with high lattice

*ishiwata@mp.es.osaka-u.ac.jp

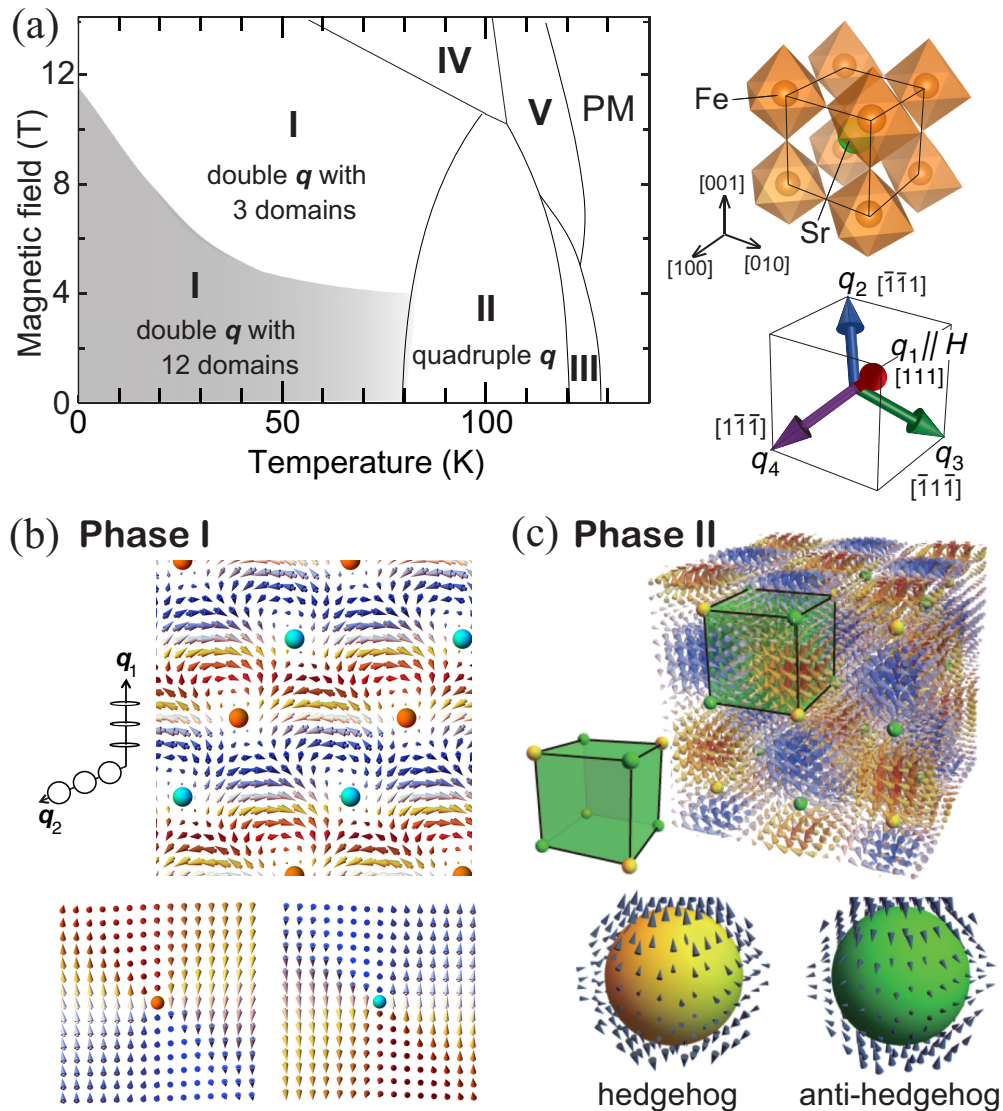


FIG. 1. (a) Magnetic phase diagram for the applied field direction along $[111]$. The shaded and the white regions in phase I correspond to states with 12 and 3 domains, respectively. The schematic crystal structure and quadruple- \mathbf{q} vectors viewed along $[111]$ are shown on the right-hand side. (b) Double- \mathbf{q} spin structure in phase I and (c) quadruple- \mathbf{q} spin structure in phase II (the color of each spin corresponds to the spin component along the direction perpendicular to both \mathbf{q}_1 and \mathbf{q}_2 for (b) and that along $[111]$ for (c), respectively). The magnified views around the singular points are shown at the bottom. Note that we adopt \mathbf{q}_1 and \mathbf{q}_2 instead of \mathbf{q}'_1 and \mathbf{q}'_2 for phase I.

symmetry [23–28]. In the absence of the DM interaction, these helimagnets have the potential to show rich topological spin textures due to fewer constraints on the spin helix. There exist a large number of centrosymmetric helimagnets, some of which show multiple- \mathbf{q} spin modulations such as the rare-earth magnets [29,30]. However, the presence of topologically nontrivial helimagnetic phases in centrosymmetric systems remains to be explored.

The simple cubic perovskite SrFeO_3 with crystal structure displayed in Fig. 1(a) is known to host a helimagnetic order below 130 K with metallic conductivity [31,32]. The origin of the helimagnetic order in SrFeO_3 and related iron oxides has been discussed in terms of the competing exchange interactions, i.e., the nearest-neighbor and further-neighbor interactions [33] or the double-exchange mechanism considering the itinerant oxygen p holes [34,35]. Early neutron diffraction

data were described in terms of a single- \mathbf{q} proper-screw spiral with the propagation vector along the $[111]$ or equivalent directions of the cubic lattice [32]. Recently, however, SrFeO_3 was shown to display a rich variety of helimagnetic phases depending on temperature and external magnetic field, as shown in Fig. 1(a) [36,37]. Among them, phases I and II are extraordinary in the sense that they exhibit a large unconventional Hall effect [36,38,39]. The presence of sharp phase transitions with unusual transport signatures indicates well-ordered magnetic superstructures, rather than an incoherent superposition of domains of the single- \mathbf{q} structure with different propagation vectors. In both phase I and phase II, the Hall resistivity as a function of \mathbf{H} along $[111]$ increases nonlinearly and reaches a maximum below the phase boundary to phase IV or phase V. While this behavior implies the emergence of noncoplanar and/or topological spin textures with scalar spin

chirality [6,7], the magnetic structures within each phase have remained elusive. In this work, on the basis of comprehensive single-crystal neutron diffraction studies, we reveal that the magnetic structures of the mysterious phases in the centrosymmetric cubic perovskite SrFeO₃ can be topological in nature, being identified as anisotropic double- \mathbf{q} and isotropic quadruple- \mathbf{q} helimagnetic structures, respectively.

II. EXPERIMENT

Single crystals of SrFeO₃ and SrFe_{0.99}Co_{0.01}O₃ were obtained by high-pressure oxygen annealing of large single crystals of the oxygen-deficient perovskite with brownmillerite-type structure as described in Refs. [36,40]. The orientation of the single crystal with dimensions of about $3 \times 3 \times 2$ mm³ was checked by x-ray Laue diffraction.

The temperature and magnetic field variations of the neutron diffraction intensities shown in Figs. 2, S3, S5, and S6 were measured for SrFeO₃ with a cold neutron time-of-flight diffractometer, WISH (Wide angle In a Single Histogram) [41,42], at the ISIS facility in the United Kingdom. The single-crystal SrFeO₃ was loaded into a vertical-field cryomagnet, whose maximum field is 13.5 T. The cubic [111] axis was set to be parallel to the magnetic field. The cryomagnet has a large vertical opening angle from -5° to 10° , which enabled us to measure the out-of-plane incommensurate magnetic reflections around the reciprocal lattice point of $(1, \bar{1}, 0)$ (Figs. 2 and S3) as well as that of $(0, 0, 0)$ (Figs. S5 and S6) under magnetic field along the [111] direction [42].

Small-angle neutron scattering (SANS) measurements were carried out for SrFe_{0.99}Co_{0.01}O₃ with a vertical-field cryomagnet (7 T at maximum) at the cold diffractometer MIRA at the German research neutron source Heinz Maier-Leibnitz FRM II, Garching, Germany [43,44], and a horizontal-field cryomagnet (6.8 T in maximum) at the SANS-I instrument at the Swiss spallation neutron source SINQ, Paul Scherrer Institute, Villigen, Switzerland. We employed an experimental setup of the horizontal configuration [see Fig. S1(a)], in which the sample can be rotated by 360° around the $[\bar{1}\bar{1}2]$ axis (ω axis), and vertical configuration [see Fig. S1(b)], in which the sample can be rotated by 360° around the [111] axis (ω axis) [42]. In both experimental configurations, the magnetic field was applied parallel to the [111] axis and perpendicular to the incident neutron beam. Experimental data taken at MIRA were collected in both polarized and unpolarized modes at a wavelength $\lambda = 4.5$ Å, and those at SANS-I were collected in the unpolarized mode at $\lambda = 4.7$ Å. For the SANS experiments, we used SrFe_{0.99}Co_{0.01}O₃ instead of SrFeO₃ because SrFe_{0.99}Co_{0.01}O₃ exhibits the same magnetic phases as SrFeO₃ but is more suitable for studying the II-V phase transition by the SANS diffractometer equipped with a spin analyzer and a cryomagnet of 7 T since its transition field is reduced below 7 T. The observed magnetic reflections are located around the reciprocal lattice point of $(0, 0, 0)$. The background of each data set was determined at high temperatures above 135 K and accordingly subtracted. The polarization of neutron spins was generated by the magnetic field gradient near the vertical superconducting magnet. The neutron flipping ratios F for the measurements at 0.3 and 7 T are 4.9 and 3.0, respectively. Here, F is related to the neutron polarization P_n by $F = (1 + P_n)/(1 - P_n)$.

III. RESULTS AND DISCUSSION

A. Multiple- \mathbf{q} helimagnetic spin structures

Figures 1(b) and 1(c) illustrate the spin structures reproduced by the superposition of the double- \mathbf{q} and quadruple- \mathbf{q} magnetic modulations, which we propose in this study as models for phases I and II, respectively. Note that we tentatively adopt the same helicity and phase for each spin modulation. Owing to the cubic symmetry of the crystal, there are four \mathbf{q} vectors: (q, q, q) , $(-q, -q, q)$, $(-q, q, -q)$, and $(q, -q, -q)$; in this paper, we refer to them as \mathbf{q}_1 , \mathbf{q}_2 , \mathbf{q}_3 , and \mathbf{q}_4 , respectively, as described in Fig. 1(a). As explained later in detail, phase I can be described as a double- \mathbf{q} structure encompassing proper-screw and cycloidal modulations with slightly different \mathbf{q} vectors, so that the overall symmetry of the superstructure is reduced [42]. As shown in Fig. 1(b), there exist singularities indicated by the blue and red circles surrounded by noncoplanar vortexlike spin configurations. On the other hand, for phase II, four equivalent proper-screw-type spin modulations yield a fcc lattice of topological singularities, at which the hedgehog (antihedgehog) spin texture acts as the source (sink) of the emergent magnetic fields [Fig. 1(c)], i.e., an emergent magnetic monopole (antimonopole). Considering the theoretical calculations in Ref. [45], the observation of the topological Hall effect in phase II is consistent with the emergence of this three-dimensional topological spin texture [22]. Here, we define the topological number as the integral of the solid angle made by the three adjacent spins around the singular point as described in Refs. [4,45]. Following this definition, the local topological numbers for the hedgehog and antihedgehog spin textures in phase II are 1 and -1 , respectively, whereas that for the singularities in phase I is not a nonzero integer. Thus, while the spin texture in phase II is topological, that in phase I might not be topological.

B. Temperature dependence of the magnetic scattering intensity

First, let us identify the multiple- \mathbf{q} state in phases I and II on the basis of results of high-resolution neutron diffraction measurements for SrFeO₃ at the WISH diffractometer at ISIS. Figure 2(a) shows integrated intensities of incommensurate magnetic reflections around the $(1, \bar{1}, 0)$ reciprocal lattice point, which were measured on heating in zero field after field cooling (FC) with an external field \mathbf{H} of 7 T along the [111] axis. The data labeled \mathbf{q}_i show the intensity corresponding to the magnetic modulation vector \mathbf{q}_i . We found that the intensity for the modulation vector of \mathbf{q}_1 at zero field was largely enhanced after the FC process with \mathbf{H} parallel to \mathbf{q}_1 as shown in Fig. 2(a). This tendency is reminiscent of a proper-screw-type magnetic order, in which a \mathbf{q} vector parallel to \mathbf{H} would be selected through the FC process due to the difference in the Zeeman energy. This is also consistent with the early neutron diffraction study proposing a simple screw-type structure [32]. However, nonzero scattering intensities are found not only for \mathbf{q}_1 but also for \mathbf{q}_{2-4} . Thus, the possibility of the single- \mathbf{q} proper-screw spin structure can be ruled out for phase I and likewise for phase II. These results suggest that the magnetic structure of phase I is a multiple- \mathbf{q} structure having at least two magnetic modulations: the major component with a proper-screw-like modulation (\mathbf{q}_1) and additional modulations (\mathbf{q}_{2-4}). Importantly, for phase I, the intensities of the reflections

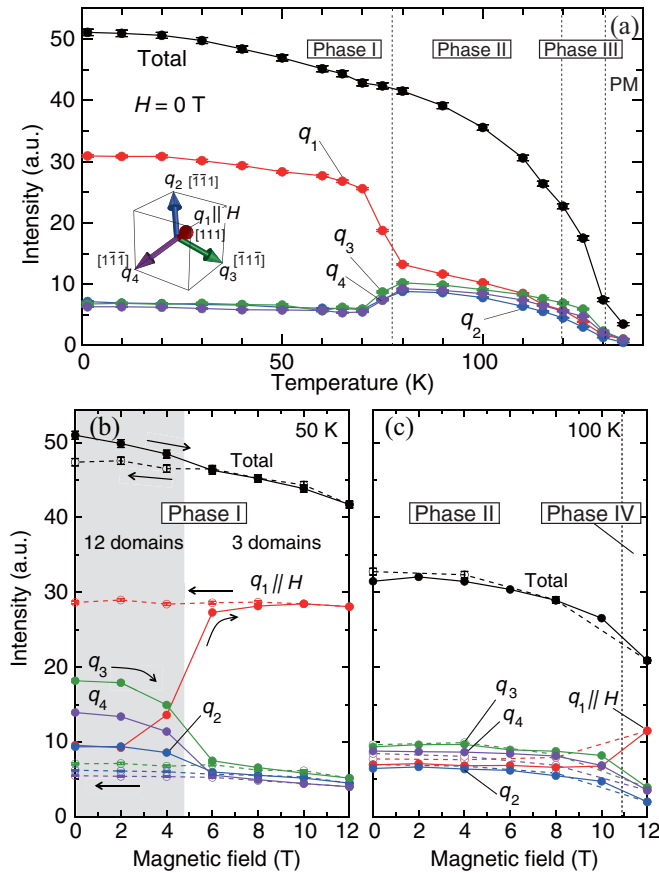


FIG. 2. (a) Temperature dependence of integrated intensities of the magnetic scattering along q_i ($i=1-4$) measured at zero field after field cooling. The total intensity for q_{1-4} is also shown. Magnetic field dependence of the magnetic scattering intensities for (b) phase I at 50 K and (c) phase II at 100 K. The data with solid lines and dashed lines were measured on increasing and decreasing the field along $[111]$, respectively. The data for (b) and (c) were measured after zero-field cooling from room temperature.

corresponding to q_2 , q_3 , and q_4 can be different from each other not only after the zero-field-cooling (ZFC) process but after the FC process (see Fig. S2 for details [42]). In other words, the threefold rotational symmetry about the $[111]$ axis is absent in phase I, reflecting the anisotropic magnetic structure allowing multidomain states under an external field along $[111]$. Therefore, we propose that phase I has the anisotropic double- q spin structure consisting of two kinds of magnetic modulations, one of which is proper-screw type. On the other hand for phase II, the scattering intensities are comparable to each other, suggesting that the field-oriented anisotropic magnetic structure in phase I disappears upon the first-order phase transition to phase II.

C. Field dependence of the magnetic scattering intensity in phases I and II

Having confirmed the multiple- q state in phases I and II, we measured the intensities of the incommensurate magnetic reflections around the $(1, -1, 0)$ reciprocal lattice point

with varying magnetic field at the selected temperatures after ZFC, as shown in Figs. 2(b) and 2(c) (for the raw data, see Fig. S3 [42]). At 50 K and zero field in phase I, the scattering intensities for q_{1-4} are distributed in a certain range, reflecting the multidomain state of the anisotropic multiple- q spin structure. As H is increased beyond 5 T, the intensity for q_1 parallel to H becomes larger, and the others become smaller. The significant H -induced change with a large hysteresis at low H is ascribable to the domain reorientation, as also suggested by the previous report on the magnetoresistance anomaly measured after ZFC [see the shaded area in Figs. 1(a) and 2(b)] [36]. Here, we would like to emphasize that the intensities for q_{2-4} never disappeared even in a magnetic field of 12 T. This is more evidence of the anisotropic double- q magnetic structure in phase I. For phase II, on the other hand, the scattering intensities for q_{1-4} are comparable to each other, and H -dependent anomalies and hysteresis are absent [see Fig. 2(c)], being consistent with the presumed isotropic quadruple- q helimagnetic structure. Upon an increase in H to 12 T that induces the II-IV phase transition, the intensity distribution tends to become the one expected for the single- q state. However, since the maximum H of 12 T is located near the phase boundary and the scattering intensities for q_{2-4} remain nonzero, further experiments with larger H are indispensable to characterize the spin structure of phase IV.

D. Direction of the helimagnetic q vectors in phases I and II

To further characterize the multiple- q spin structure and the domain state in phase I, we measured SANS for q_1 and q_2 after FC and ZFC. The SANS experiments were performed for $\text{SrFe}_{0.99}\text{Co}_{0.01}\text{O}_3$ with essentially the same phase diagram as SrFeO_3 [see Fig. 4(a) below] [46], while the magnitudes of the q vectors of $\text{SrFe}_{0.99}\text{Co}_{0.01}\text{O}_3$ are about 8% smaller than that of SrFeO_3 . Figure 3(e) shows the magnetic reflections around q_1 as functions of $\Delta\chi$ and $\Delta\omega$ measured at 3 K after FC. Here, $\Delta\chi$ and $\Delta\omega$ correspond to the relative angles from $[111]$ to vertical and horizontal directions, respectively, in the horizontal configuration [see Fig. 3(a)]. The intensity of the profile at selected $\Delta\chi$ and $\Delta\omega$ is obtained by the integration as a function of the momentum transfer vector Q in the range $0.28 \leq |Q| \leq 0.38$ (for details, see Fig. S4 [42]). The scattering profile for q_1 revealed that the magnetic modulation wave vector is no longer described by the simple (q, q, q) but split into three peaks indexed as (q, q, q') ($=q'_{1(2)}$), (q, q', q) ($=q'_{1(3)}$) and (q', q, q) ($=q'_{1(4)}$), where $q \simeq 0.114$ (r.l.u.) and $q' \simeq 0.123$ (r.l.u.) (r.l.u. denotes reciprocal lattice unit). The observation of the triplet peaks around q_1 after FC with H parallel to $[111]$ is a signature of the three q -dependent domains (for details, see Fig. S2 [42]). On the other hand, for q_2 in Fig. 3(g), a single peak is found at a position slightly shifted from the $[\bar{1}11]$ direction, which is assigned to be $(-q, -q, q')$ ($=q'_{2(1)}$). The azimuthal directions of these propagation vectors deviate from the $\langle 111 \rangle$ equivalents, so that the double- q state in phase I can accommodate the angular mismatch between the two q vectors. As the temperature increases through the I-II phase transition at 90 K, the directions of all propagation vectors become parallel to the $\langle 111 \rangle$ equivalents, consistent with the proposal for the

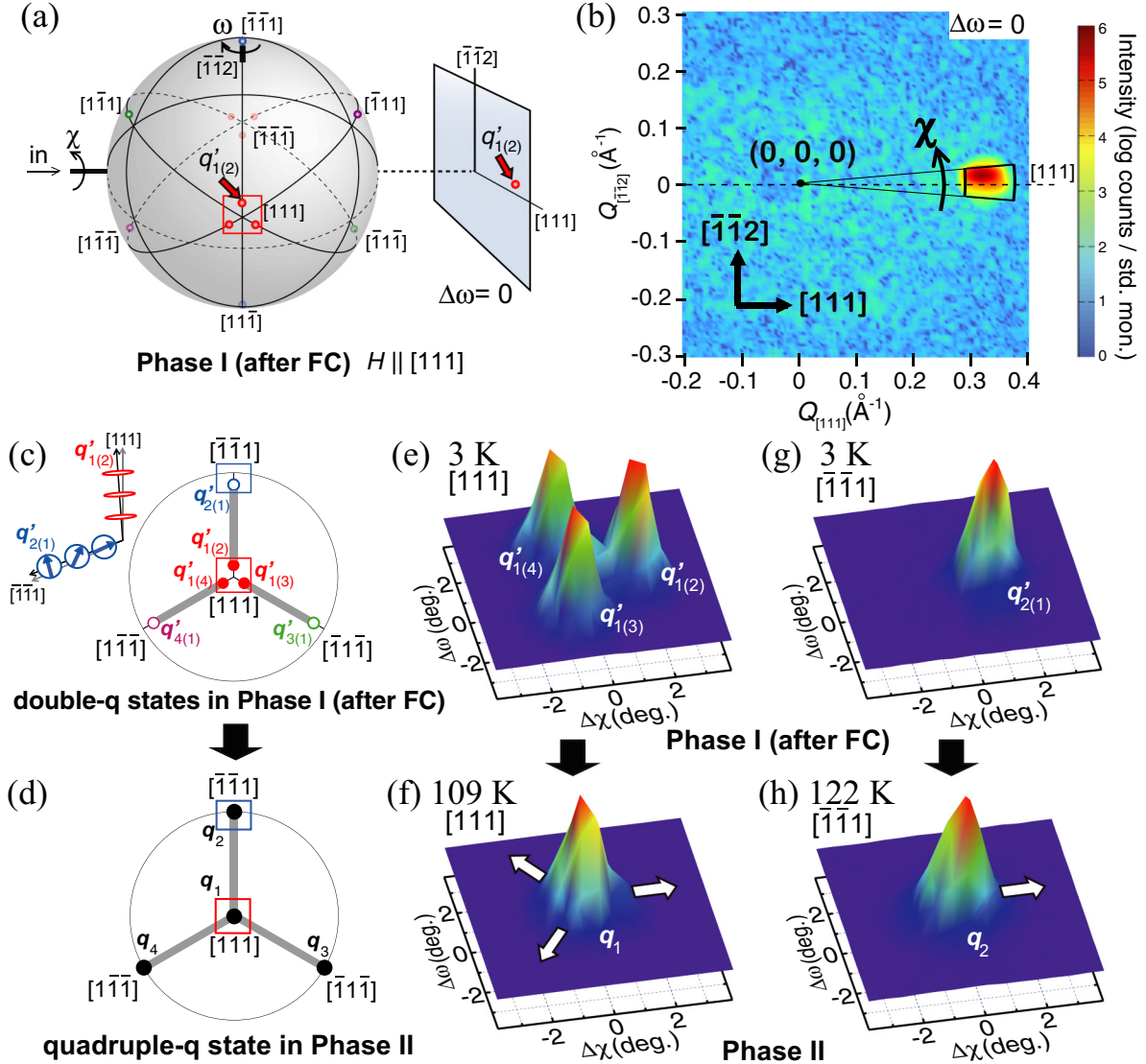


FIG. 3. (a) Schematic representation describing the crystallographic directions and the azimuthal positions of magnetic scattering peaks in the horizontal configuration for phase I after field cooling (FC). The three red balls indicated by the red square on the gray sphere correspond to the triplet magnetic scattering peaks deviating by 2° from the $[111]$ direction. (b) SANS data measured at 3 K with the relative rocking angle $\Delta\omega = 0$. The observed magnetic reflection corresponds to the helimagnetic modulation $q'_{1(2)}$, which is indicated by the red arrow in the (a). Stereographic projections of magnetic scattering peaks in (c) phase I after field cooling and (d) phase II. The solid and open circles represent the magnetic reflections for the proper-screw and vertical-cycloid-type spin propagations, respectively. (e) and (f) Integrated magnetic scattering profiles around q_1 parallel to $[111]$. The peaks in (e) and (g) correspond to the triplet red solid circles and a single blue open circle in the (c), respectively. (g) and (h) Integrated magnetic scattering profiles around q_2 parallel to $[\bar{1}\bar{1}\bar{1}]$. The intensity is normalized by the largest value. The data were collected on heating in zero field after field cooling under a magnetic field of 6.8 T for $\text{SrFe}_{0.99}\text{Co}_{0.01}\text{O}_3$. The data in (b), (e), and (f) were collected with the horizontal configuration, and those in (g) and (h) were collected with the vertical configuration (see Fig. S1 [42]).

isotropic quadruple- q helimagnetic structure in phase II [see Figs. 3(d), 3(f) and 3(h)]. The schematic representations of the observed scattering peaks for phases I and II are displayed in Figs. 3(c) and 3(d), respectively. The numbers of the domain types of phase I after ZFC and FC states are 12 and 3, respectively, the latter of which is obtained by considering the threefold symmetry around $[111]$ (we ignored the helicity degree of freedom for the consideration of the domain types.). At least at low temperature, magnetic fields of order ~ 10 T therefore mostly select different equivalent domains without modifying the magnetic structure substantially. In contrast to

the present system showing distinct q -dependent domains, the helimagnetic q vectors in MnSi can be continuously reoriented towards the field direction by small magnetic fields of 0.1 T [47], which presumably reflects the difference in the magnetic anisotropy or the helimagnetic period (18 nm for MnSi and 1.8 nm for SrFeO_3).

E. Polarized small-angle neutron scattering

Next, we performed polarized SANS experiments to learn microscopically how the spins are modulating along q'_2 or q_2 after the FC process with H along $[111]$. Here, we assume

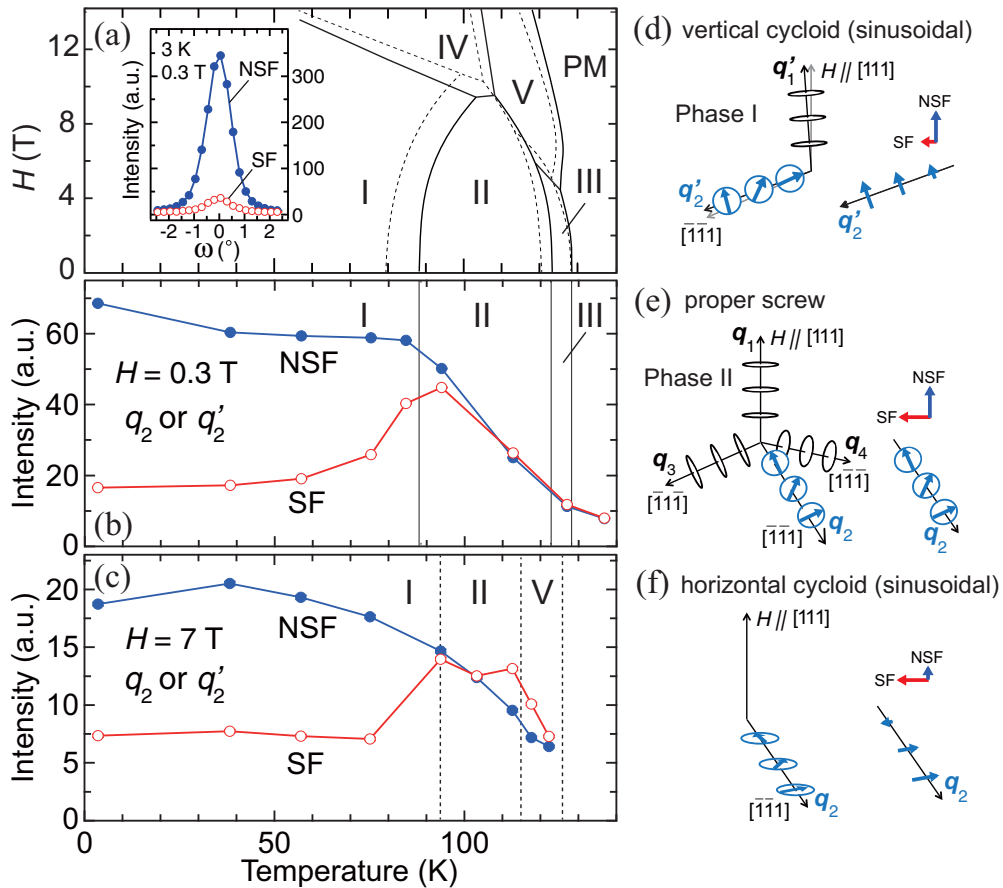


FIG. 4. (a) The magnetic phase diagram of $\text{SrFe}_{0.99}\text{Co}_{0.01}\text{O}_3$ reproduced from [46], on which the magnetic phase diagram of SrFeO_3 is superimposed (the phase boundary of SrFeO_3 is shown by dashed lines). The integrated neutron scattering intensities as a function of $\Delta\omega$ at 3 K and 0.3 T for spin-flip (SF) and non-spin-flip (NSF) geometries are shown in the inset. All the data were collected after field cooling in a magnetic field of 7 T. Temperature dependence of SF and NSF scattering intensities measured on heating at (b) 0.3 T and (c) 7 T. In each case, the applied magnetic field and the incident neutron spin are parallel to [111]. Schematic illustrations of the spiral spin propagation for \mathbf{q}'_2 or \mathbf{q}_2 with (d) vertical-cycloid-type (phase I), (e) proper-screw-type (phase II), and (f) horizontal-cycloid-type configurations, where the right-hand side shows the effective spin components for spin-polarized SANS.

three possible arrangements of spin modulation: (i) vertical-cycloid (-sinusoidal) type with spins on the plane parallel to \mathbf{q}'_2 and \mathbf{H} [Fig. 4(d)], (ii) proper-screw type with spins on the plane normal to \mathbf{q}_2 [Fig. 4(e)], and (iii) horizontal-cycloid (-sinusoidal) type with spins on the plane parallel to \mathbf{q}_2 and normal to \mathbf{H} [Fig. 4(f)]. Since only the component of the magnetic moments perpendicular to the scattering vector cause neutron scattering, the spin components contributing to the scattering intensity can be described as shown on the right side of Figs. 4(d)–4(f). In the polarized SANS measurements, since the non-spin-flip (NSF) and the spin-flip (SF) geometries detect only the spin components parallel and normal to \mathbf{H} , respectively, the intensity ratios of NSF and SF scattering at \mathbf{q}'_2 or \mathbf{q}_2 are expected to display the dependence represented by the relative lengths of the blue and red arrows in Figs. 4(d)–4(f). From the intensity ratios, we can distinguish between the three types of spin spirals shown on the left side of Figs. 4(d)–4(f), while we cannot rule out the possibility that the sinusoidal spin modulations shown on the right side of Figs. 4(d) and 4(f) are proper models. The measurements were performed after FC in phase I, so that three kinds of domains with \mathbf{q}'_1 nearly parallel

to \mathbf{H} are selected. The inset of Fig. 4(a) shows the ω -scan profiles of the magnetic scattering for \mathbf{q}'_2 at 3 K and 0.3 T, which were normalized by the flipping ratios. As shown in Figs. 4(b) and 4(c), the normalized scattering intensity for the NSF geometry is much larger than that for the SF geometry in phase I, whereas the scattering intensities for both geometries are nearly the same in phase II. This result indicates that phase I and phase II encompass vertical-cycloid and proper-screw states, respectively, propagating along $[\bar{1}\bar{1}1]$, which is consistent with the fact that the magnetic scattering intensity along [111] is much larger than those along the other $\langle 111 \rangle$ equivalents after FC in phase I, which is not the case for phase II [see Fig. 2(a)]. In phase V at 7 T, the scattering intensity for the SF geometry is larger than that for the NSF geometry, implying that the spin arrangement propagating along $[\bar{1}\bar{1}1]$ is in the horizontal-cycloid type [see Fig. 4(f)]. It should be noted here that each multiple- \mathbf{q} spin spiral is expected to have a ferromagnetic component induced by external magnetic fields, which cannot be confirmed in this work. Thus, it is reasonable to assume that phase V has multiple- \mathbf{q} spin spirals as well, but further experiments are required to identify the detailed spin structure.

IV. CONCLUSIONS

To summarize, we have identified two kinds of multiple- q spin structures in SrFeO₃ that appear robustly even without external magnetic fields. The anisotropic double- q spin structure in phase I manifests itself as a nontrivial order, reflecting the versatility of the centrosymmetric lattice that permits various types of spin spirals. However, this spin texture cannot explain the observed topological Hall resistivity because the expected direction of the emergent magnetic flux is perpendicular to the external magnetic field. Future research will have to assess whether the discrepancy between the expected and observed directions of the emergent magnetic flux in phase I arises from an additional internal spin modulation that is not resolved in the current experiment. On the other hand, phase II can be described in terms of a topologically nontrivial order with an isotropic quadruple- q spin spiral that presumably yields emergent magnetic monopoles as reported for the noncentrosymmetric helimagnet MnGe characterized by an orthogonal triple- q spiral [21].

We now turn to the mechanisms underlying the observed cascade of magnetic phase transitions. The fact that the diffraction patterns at the lowest temperature in ZFC and FC states are very similar implies that phase I is not stabilized by the Zeeman interaction, but rather by anisotropic terms in the zero-field spin Hamiltonian (such as magnetocrystalline anisotropies generated by the spin-orbit coupling) that go beyond the primary isotropic double-exchange and/or superexchange interactions. With increasing temperature, the corresponding free-energy gain could be offset by the higher entropy of the more symmetric quadruple- q structure, leading to the observed phase transition between phases I and II. Recently, Monte Carlo simulations based on a Kondo lattice model with a biquadratic interaction defined in momentum space indicated various multiple- q phases on a centrosymmetric lattice with rotational symmetry [28]. Although this model does not apply directly to our system, this theoretical work and

our experimental results provide a timely showcase of the rich variety of multiple- q helimagnetic phases with topological singularities that can be expected to emerge ubiquitously in frustrated itinerant magnets with high lattice symmetry, even without the DM interaction. Moreover, perovskite-type oxides are a broad class of materials that already have many applications, especially in the form of heterostructures enabling the interplay between topological magnetism and other collective quantum phenomena. The discovery of topological spin order in SrFeO₃ is therefore a milestone for integrating potential topological magnetic states into existing device architectures.

ACKNOWLEDGMENTS

The authors thank M. Mostovoy, S. Hayami, Y. Motome, N. Nagaosa, and M. Takano for useful comments and thank N. Egetenmeyer for her kind experimental support. This work is partly supported by Grants-in-Aid for Scientific Research, Japan Society for the Promotion of Science, Japan (Kakenhi Grants No. 17H01195 and No. 16K17736), JST PRESTO Hyper-nano-space design toward Innovative Functionality (Grant No. JPMJPR1412), and the Asahi Glass Foundation. D.S.I. acknowledges support from the German Research Foundation (DFG) through project C03 of the Collaborative Research Center SFB 1143 in Dresden (Project No. 247310070) and the Würzburg-Dresden Cluster of Excellence “ct.qmat” (EXC 2147, Project No. 39085490). J.S.W. acknowledges support from the Swiss National Science Foundation (SNSF) via the Sinergia network “NanoSkyrmionics” (Grant No. CRSII5-171003), and the SNSF project Grant No. 200021-153451. B.K. acknowledges support from the DFG through the Collaborative Research Center TRR80 (Project No. 107745057). Y.W.L. acknowledges support from the MOST-RIKEN collaboration project (Grant No. 2018YFE0103200).

-
- [1] A. Bogdanov and A. Hubert, Thermodynamically stable magnetic vortex states in magnetic crystals, *J. Magn. Magn. Mater.* **138**, 255 (1994).
- [2] U. K. Röbler, A. N. Bogdanov, and C. Pfleiderer, Spontaneous skyrmion ground states in magnetic metals, *Nature (London)* **442**, 797 (2006).
- [3] S. Mühlbauer, B. Binz, F. Jonietz, C. Pfleiderer, A. Rosch, A. Neubauer, R. Georgii, and P. Böni, Skyrmion lattice in a chiral magnet, *Science* **323**, 915 (2009).
- [4] N. Nagaosa and Y. Tokura, Topological properties and dynamics of magnetic skyrmions, *Nat. Nanotechnol.* **8**, 899 (2013).
- [5] N. Kanazawa, S. Seki, and Y. Tokura, Noncentrosymmetric magnets hosting magnetic skyrmions, *Adv. Mater.* **29**, 1603227 (2017).
- [6] A. Neubauer, C. Pfleiderer, B. Binz, A. Rosch, R. Ritz, P. G. Niklowitz, and P. Böni, Topological Hall Effect in the A Phase of MnSi, *Phys. Rev. Lett.* **102**, 186602 (2009).
- [7] N. Kanazawa, Y. Onose, T. Arima, D. Okuyama, K. Ohoyama, S. Wakimoto, K. Kakurai, S. Ishiwata, and Y. Tokura, Large Topological Hall Effect in a Short-Period Helimagnet MnGe, *Phys. Rev. Lett.* **106**, 156603 (2011).
- [8] F. Jonietz, S. Mühlbauer, C. Pfleiderer, A. Neubauer, W. Münzer, A. Bauer, T. Adams, R. Georgii, P. Böni, R. A. Duine, K. Everschor, M. Garst, and A. Rosch, Spin transfer torques in MnSi at ultralow current densities, *Science* **330**, 1648 (2010).
- [9] M. Mochizuki, X. Z. Yu, S. Seki, N. Kanazawa, W. Koshibae, J. Zang, M. Mostovoy, Y. Tokura, and N. Nagaosa, Thermally driven ratchet motion of a skyrmion microcrystal and topological magnon Hall effect, *Nat. Mater.* **13**, 241 (2014).
- [10] X. Z. Yu, Y. Onose, N. Kanazawa, J. H. Park, J. H. Han, Y. Matsui, N. Nagaosa, and Y. Tokura, Real-space observation of a two-dimensional skyrmion crystal, *Nature (London)* **465**, 901 (2010).
- [11] W. Münzer, A. Neubauer, T. Adams, S. Mühlbauer, C. Franz, F. Jonietz, R. Georgii, P. Böni, B. Pedersen, M. Schmidt, A. Rosch, and C. Pfleiderer, Skyrmion lattice in the doped semiconductor Fe_{1-x}Co_xSi, *Phys. Rev. B* **81**, 041203(R) (2010).

- [12] X. Z. Yu, N. Kanazawa, Y. Onose, K. Kimoto, W. Z. Zhang, S. Ishiwata, Y. Matsui, and Y. Tokura, Near room-temperature formation of a skyrmion crystal in thin-films of the helimagnet FeGe, *Nat. Mater.* **10**, 106 (2011).
- [13] S. Seki, X. Z. Yu, S. Ishiwata, and Y. Tokura, Observation of skyrmions in a multiferroic material, *Science* **336**, 198 (2012).
- [14] Y. Tokunaga, X. Z. Yu, J. S. White, H. M. Rønnow, D. Morikawa, Y. Taguchi, and Y. Tokura, A new class of chiral materials hosting magnetic skyrmions beyond room temperature, *Nat. Commun.* **6**, 7638 (2015).
- [15] I. Kézsmárki, S. Bordács, P. Milde, E. Neuber, L. M. Eng, J. S. White, H. M. Rønnow, C. D. Dewhurst, M. Mochizuki, K. Yanai, H. Nakamura, D. Ehlers, V. Tsurkan, and A. Loidl, Néel-type skyrmion lattice with confined orientation in the polar magnetic semiconductor GaV₄S₈, *Nat. Mater.* **14**, 1116 (2015).
- [16] Y. Fujima, N. Abe, Y. Tokunaga, and T. Arima, Thermodynamically stable skyrmion lattice at low temperatures in a bulk crystal of lacunar spinel GaV₄Se₈, *Phys. Rev. B* **95**, 180410(R) (2017).
- [17] S. Bordács, A. Butykai, B. G. Szigeti, J. S. White, R. Cubitt, A. O. Leonov, S. Widmann, D. Ehlers, H.-A. Krug von Nidda, V. Tsurkan, A. Loidl, and I. Kézsmárki, Equilibrium skyrmion lattice ground state in a polar easy-plane magnet, *Sci. Rep.* **7**, 7584 (2017).
- [18] T. Kurumaji, T. Nakajima, V. Ukleev, A. Feoktystov, T. Arima, K. Kakurai, and Y. Tokura, Néel-Type Skyrmion Lattice in the Tetragonal Polar Magnet VOSe₂O₅, *Phys. Rev. Lett.* **119**, 237201 (2017).
- [19] A. K. Nayak, V. Kumar, T. Ma, P. Werner, E. Pippel, R. Sahoo, F. Damay, U. K. Rößler, C. Felser, and S. S. P. Parkin, Magnetic antiskyrmions above room temperature in tetragonal Heusler materials, *Nature (London)* **548**, 561 (2017).
- [20] S. Heinze, K. von Bergmann, M. Menzel, J. Brede, A. Kubetzka, R. Wiesendanger, G. Bihlmayer, and S. Blügel, Spontaneous atomic-scale magnetic skyrmion lattice in two dimensions, *Nat. Phys.* **7**, 713 (2011).
- [21] N. Kanazawa, J.-H. Kim, D. S. Inosov, J. S. White, N. Egetenmeyer, J. L. Gavilano, S. Ishiwata, Y. Onose, T. Arima, B. Keimer, and Y. Tokura, Possible skyrmion-lattice ground state in the B20 chiral-lattice magnet MnGe as seen via small-angle neutron scattering, *Phys. Rev. B* **86**, 134425 (2012).
- [22] N. Kanazawa, Y. Nii, X.-X. Zhang, A. S. Mishchenko, G. De Filippis, F. Kagawa, Y. Iwasa, N. Nagaosa, and Y. Tokura, Critical phenomena of emergent magnetic monopoles in a chiral magnet, *Nat. Commun.* **7**, 11622 (2016).
- [23] T. Okubo, S. Chung, and H. Kawamura, Multiple- q States and the Skyrmion Lattice of the Triangular-Lattice Heisenberg Antiferromagnet under Magnetic Fields, *Phys. Rev. Lett.* **108**, 017206 (2012).
- [24] A. O. Leonov and M. Mostovoy, Multiply periodic states and isolated skyrmions in an anisotropic frustrated magnet, *Nat. Commun.* **6**, 8275 (2015).
- [25] Z. Wang, Y. Kamiya, A. H. Nevidomskyy, and C. D. Batista, Three-Dimensional Crystallization of Vortex Strings in Frustrated Quantum Magnets, *Phys. Rev. Lett.* **115**, 107201 (2015).
- [26] C. D. Batista, S.-Z. Lin, S. Hayami, and Y. Kamiya, Frustration and chiral orderings in correlated electron systems, *Rep. Prog. Phys.* **79**, 084504 (2016).
- [27] R. Ozawa, S. Hayami, K. Barros, G.-W. Chern, Y. Motome, and C. D. Batista, Vortex crystals with chiral stripes in itinerant magnets, *J. Phys. Soc. Jpn.* **85**, 103703 (2016).
- [28] S. Hayami, R. Ozawa, and Y. Motome, Effective bilinear-biquadratic model for noncoplanar ordering in itinerant magnets, *Phys. Rev. B* **95**, 224424 (2017).
- [29] E. M. Forgan, E. P. Gibbons, K. A. McEwen, and D. Fort, Observation of a Quadruple- q Magnetic Structure in Neodymium, *Phys. Rev. Lett.* **62**, 470 (1989).
- [30] J. Jensen and A. R. Mackintosh, *Rare Earth Magnetism: Structures and Excitations* (Oxford University Press, Oxford, 1991).
- [31] J. B. MacChesney, R. C. Sherwood, and J. F. Potter, Electric and magnetic properties of the strontium ferrates, *J. Chem. Phys.* **43**, 1907 (1965).
- [32] T. Takeda, Y. Yamaguchi, and H. Watanabe, Magnetic structure of SrFeO₃, *J. Phys. Soc. Jpn.* **33**, 967 (1972).
- [33] J.-H. Kim, A. Jain, M. Reehuis, G. Khaliullin, D. C. Peets, C. Ulrich, J. T. Park, E. Faulhaber, A. Hoser, H. C. Walker, D. T. Adroja, A. C. Walters, D. S. Inosov, A. Maljuk, and B. Keimer, Competing Exchange Interactions on the Verge of a Metal-Insulator Transition in the Two-Dimensional Spiral Magnet Sr₃Fe₂O₇, *Phys. Rev. Lett.* **113**, 147206 (2014).
- [34] M. Mostovoy, Helicoidal Ordering in Iron Perovskites, *Phys. Rev. Lett.* **94**, 137205 (2005).
- [35] M. Azhar and M. Mostovoy, Incommensurate Spiral Order from Double-Exchange Interactions, *Phys. Rev. Lett.* **118**, 027203 (2017).
- [36] S. Ishiwata, M. Tokunaga, Y. Kaneko, D. Okuyama, Y. Tokunaga, S. Wakimoto, K. Kakurai, T. Arima, Y. Taguchi, and Y. Tokura, Versatile helimagnetic phases under magnetic fields in cubic perovskite SrFeO₃, *Phys. Rev. B* **84**, 054427 (2011).
- [37] M. Reehuis, C. Ulrich, A. Maljuk, Ch. Niedermayer, B. Ouladdiaf, A. Hoser, T. Hofmann, and B. Keimer, Neutron diffraction study of spin and charge ordering in SrFeO_{3- δ} , *Phys. Rev. B* **85**, 184109 (2012).
- [38] N. Hayashi, T. Terashima, and M. Takano, Oxygen-holes creating different electronic phases in Fe⁴⁺-oxides: Successful growth of single crystalline films of SrFeO₃ and related perovskites at low oxygen pressure, *J. Mater. Chem.* **11**, 2235 (2001).
- [39] S. Chakraverty, T. Matsuda, H. Wadati, J. Okamoto, Y. Yamasaki, H. Nakao, Y. Murakami, S. Ishiwata, M. Kawasaki, Y. Taguchi, Y. Tokura, and H. Y. Hwang, Multiple helimagnetic phases and topological Hall effect in epitaxial thin films of pristine and Co-doped SrFeO₃, *Phys. Rev. B* **88**, 220405(R) (2013).
- [40] Y. W. Long, Y. Kaneko, S. Ishiwata, Y. Taguchi, and Y. Tokura, Synthesis of cubic SrCoO₃ single crystal and its anisotropic magnetic and transport properties, *J. Phys.: Condens. Matter* **23**, 245601 (2011).
- [41] L. C. Chapon, P. Manuel, P. G. Radaelli, C. Benson, L. Perrott, S. Ansell, N. J. Rhodes, D. Raspino, D. Duxbury, E. Spill, and J. Norris, Wish: The new powder and single crystal magnetic diffractometer on the second target station, *Neutron News* **22**, 22 (2011).
- [42] See Supplemental Material at <http://link.aps.org/supplemental/10.1103/PhysRevB.101.134406> for the details of neutron measurements and the domain state of the double- q helimagnetic structure in phase I. In addition, raw data for WISH experiments and SANS experiments are shown.

- [43] R. Georgii and K. Seemann, MIRA: Dual wavelength band instrument, *J. Large-Scale Res. Facil.* **1**, A3 (2015).
- [44] R. Georgii, T. Weber, G. Brandl, M. Skoulatos, M. Janoschek, S. Mühlbauer, C. Pfleiderer, and P. Böni, The multi-purpose three-axis spectrometer (TAS) MIRA at FRM II, *Nucl. Instrum. Methods Phys. Res., Sect. A* **881**, 60 (2018).
- [45] J. H. Park and J. H. Han, Zero-temperature phases for chiral magnets in three dimensions, *Phys. Rev. B* **83**, 184406 (2011).
- [46] Y. W. Long, Y. Kaneko, S. Ishiwata, Y. Tokunaga, T. Matsuda, H. Wadati, Y. Tanaka, S. Shin, Y. Tokura, and Y. Taguchi, Evolution of magnetic phases in single crystals of $\text{SrFe}_{1-x}\text{Co}_x\text{O}_3$ solid solution, *Phys. Rev. B* **86**, 064436 (2012).
- [47] A. Bauer, A. Chacon, M. Wagner, M. Halder, R. Georgii, A. Rosch, C. Pfleiderer, and M. Garst, Symmetry breaking, slow relaxation dynamics, and topological defects at the field-induced helix reorientation in MnSi, *Phys. Rev. B* **95**, 024429 (2017).